Spectral-Based Color Separation Using Linear Regression Iteration

Philipp Urban,[1]* Rolf-Rainer Grigat[2]

[1] Ratio Entwicklungen GmbH, Hamburg University of Technology, Harburger Schlosstrasse 20, 21079 Hamburg, Germany

[2] Vision Systems, Hamburg University of Technology, Harburger Schlosstrasse 20, 21079 Hamburg, Germany

Received 18 July 2005; accepted 26 October 2005

Abstract: The present article will introduce a very simple new method for spectral-based color separation. This method inverts a Yule–Nielsen modified spectral Neugebauer model, utilizing its affine multilinearity in the $1/n$*-space. By means of linear regression, a sequence of colorant combinations is constructed converging to a colorant combination that approximates the desired reflectance spectrum in the sense of the smallest RMS error. Each iteration step consists mainly of two simple matrix–vector multiplications. With the aid of various simulation experiments, investigations on the speed of convergence are conducted.*© 2006 Wiley Periodicals, Inc. Col Res Appl, 31, 229–239, 2006; Published online in Wiley InterScience (www.interscience.wiley.com). DOI 10.1002/col.20211

Key words: printing; spectral reproduction; separation; inversion of spectral models

INTRODUCTION

In recent years various spectral models were developed to estimate the behavior of color printers.[1–8] These so-called "forward models" predict the reflectance spectrum for each colorant mixture that is used by the printer. A good overview of many of these models is given by Wybel and Berns.[9] Particularly effective was the Yule–Nielsen modified spectral Neugebauer (YNSN) model, which, despite its simplicity, yields very low error rates.[9,10] Effects such as optical dot gain are modeled using an n-factor to be chosen by empirical means.

To reproduce multispectral images by a printer, suitable control values must be found for a given reflectance spectrum. This corresponds exactly to the inverse process, which is also termed a "backward model." Unfortunately, analytical inversion of the forward models is generally not possible. An additional problem is the physical limitation of the device. For reflectance spectra not reproducible by a printer, an alternative spectrum from the spectral gamut is sought that, in terms of a metric (cf., e.g.,11), has the smallest distance to the predetermined spectrum. This corresponds to the solution of a constrained optimization problem that minimizes the YNSN model error on the colorant cube with respect to this metric. Zuffi and Schettini[12] used the Levenberg–Marquardt method to invert the YNSN model. Taplin[13] compared various standard methods for numerical optimization (cf. 14), including a quasi-Newton method, a method with conjugated gradients, and Powell's multidimensional successive-line-minimization method as well as a Simplex method. Tzeng *et al.*[15,16] used both a Newton–Raphson method and a Simplex method for separation.

Popular methods for numerical inversion or numerical optimization are based on Newton-like methods (e.g., Gauss–Newton, Levenberg–Marquardt). These methods have a high convergence order near the solution, which is quadratic in the case of the Newton method. A drawback of these methods is the necessary calculation and evaluation of the Jacobi matrix or, in the case of an optimization, of the Hesse matrix, as well as the solution of a linear equation system for each iteration step. A further drawback is the fact that these methods do not accommodate constraints. The sought effective area coverages of the colorants must lie in the range of 0–100%; however, requiring a modification of the methods, which is at the cost of the high convergence order. Such a modification could, for example, consist of a clipping after each iteration step (cf. 12). However, the so-modified method does not converge necessarily, particularly if the solution lies on the boundary of the colorant cube. Another possible modification for accommodating the relatively simple linear constraints is the so-called *Active Set Method,* described, by way of example, in Ref. 17.

* Correspondence to: P. Urban (e-mail: urban@tu-harburg.de)

The method presented in this article for inversion of the YNSN model requires neither an evaluation of the Jacobi, or Hesse matrix, nor solution of a linear equation system. Each iteration step needs only two simple matrix–vector multiplications (cf. Appendix B). Convergence is ensured for any arbitrary start value within the colorant cube. This article is to enable the reader to implement, with the simplest of means, a robust algorithm for the inversion of the YNSN model.

This article is structured as follows: The first section introduces the YNSN model, explaining the significance of its model parameters. The next is dedicated to the inversion of the YNSN model. Here, using a model algorithm much employed in optimization, the **LRI** method is developed. The compact algorithm of the **LRI** method is presented. Design of various simulation experiments are presented in the Experiments section. Then Results and Discussion follow with the focus primarily on the speed of convergence. In Conclusion, a summary is given. Appendix A examines the mathematical background, while Appendix B contains a complexity estimation and a few recommendations for implementation.

YULE–NIELSEN MODIFIED SPECTRAL NEUGEBAUER MODEL

The YNSN model is one of the most popular models for the prediction of the reflectance spectrum produced by a printer, with a special colorant control. It can be adjusted to a relatively small amount of necessary measurements.

The plain Neugebauer model[2] is an expansion of the Murray–Davies model[1] for CMY multicolor printing. For this the reflectance spectra of the eight so-called Neugebauer primaries must be measured. These consist of the plain substrate, i.e., white $R_{1,\lambda}$, the colorants cyan $R_{2,\lambda}$, magenta $R_{3,\lambda}$, and yellow $R_{4,\lambda}$, the overlapping of two colorants into red $R_{5,\lambda}$, green $R_{6,\lambda}$, and blue $R_{7,\lambda}$, and the overlapping of all colorants into black $R_{8,\lambda}$. Given uniform distribution of the dots on the substrate, the percentage of effective area coverage of the Neugebauer primaries may be computed through the effective area coverages ψ_c, ψ_m, $\psi_y \in [0, 1]$ of the colorants by means of the so-called Demichel equations:

$$
\begin{aligned}
&\text{White} && a_1(\psi_c, \psi_m, \psi_y) = (1-\psi_c)(1-\psi_m)(1-\psi_y)\\
&\text{Cyan} && a_2(\psi_c, \psi_m, \psi_y) = \psi_c(1-\psi_m)(1-\psi_y)\\
&\text{Magenta} && a_3(\psi_c, \psi_m, \psi_y) = (1-\psi_c)\psi_m(1-\psi_y)\\
&\text{Yellow} && a_4(\psi_c, \psi_m, \psi_y) = (1-\psi_c)(1-\psi_m)\psi_y\\
&\text{Red} && a_5(\psi_c, \psi_m, \psi_y) = (1-\psi_c)\psi_m\psi_y\\
&\text{Green} && a_6(\psi_c, \psi_m, \psi_y) = \psi_c(1-\psi_m)\psi_y\\
&\text{Blue} && a_7(\psi_c, \psi_m, \psi_y) = \psi_c\psi_m(1-\psi_y)\\
&\text{Black} && a_8(\psi_c, \psi_m, \psi_y) = \psi_c\psi_m\psi_y.
\end{aligned}
\tag{1}
$$

The effective colorant area coverages used here must not be confused with the theoretical area coverages, which correspond to the control values of the printer. An exact definition of terms, as well as a calculation formula of the effective area coverage from the corresponding reflectance spectra, is given, by way of example, in Ref. 9. In practice, the effective area coverages of each colorant can be assigned to the theoretical area coverages via an invertible, one-dimensional lookup table. Knowledge of the effective area coverages thus implies control of the printer via the theoretical area coverages. In the following we shall therefore limit ourselves to the effective area coverages, which, for each colorant, will be normalized to the interval [0, 1].

Where the colorants cyan, magenta, and yellow have the effective area coverages ψ_c, ψ_m, and ψ_y, the resulting reflectance spectrum can be approximated via the spectral Neugebauer equation

$$
R_\lambda(\psi_c, \psi_m, \psi_y) = \sum_{i=1}^{8} a_i(\psi_c, \psi_m, \psi_y)\, R_{i,\lambda}. \tag{2}
$$

If the printer has more than three colorants, the model can simply be expanded as the Demichel equations (1) are nothing more than the "weights" of the trilinear interpolation of the Neugebauer primaries. Where there are m colorants, the number of Neugebauer primaries increases to 2^m and the proportional area coverages can be determined via the weights of the multilinear interpolation.

One effect that is not taken into consideration by the plain Neugebauer model is the so-called optical dot gain. The optical dot gain or *Yule–Nielsen Effect*[3] describes the scattering behavior of photons penetrating into the substrate (colorants and paper). This way light can penetrate into the plain paper, scattering under the color dots or vice versa, giving the impression of a halo that makes the color dot appear larger than it actually is. This effect can be modeled by expansion of the Neugebauer model via the empirical Yule–Nielsen n-factor.

Investigations on the optical dot gain and the Yule–Nielsen n-factor may be gathered from other publications.[18–21]

The general YNSN model for a printer with m colorants, the Neugebauer primaries $R_{i,\lambda}$, $i = 1, \ldots, 2^m$, and the effective area coverages $\psi = (\psi_1, \ldots, \psi_m)^T \in [0, 1]^m$ takes the form

$$
R_\lambda(\psi) = \left[\sum_{i=1}^{2^m} a_i(\psi)\, R_{i,\lambda}^{1/n} \right]^n. \tag{3}
$$

Further reduction of the error rates can be achieved if the n-factor is chosen as a function of the wavelength (cf. 22, 23) or a regression of the Neugebauer primaries is conducted as in Ref. 24.

Methods for the adjustment of the YNSN model, i.e., of the effective area coverages and of the Yule–Nielsen n-factor, to the measurement data can be gathered, for example, from Ref. 22.

As already indicated in the Introduction, exact reproduction of a predetermined reflectance spectrum is not always possible so that a reflectance spectrum must be generated from the spectral gamut, which, according to a special metric, has the smallest distance to the spectrum submitted. For the Euclidean norm, this requirement results in the following constrained optimization problem.

Problem 1.
Solve

$$F(\psi) := \|R_\lambda(\psi) - r_\lambda\|_2^2 \stackrel{!}{=} \min \tag{4}$$

with the constraint

$$\psi \in [0, 1]^m. \tag{5}$$

An analytical solution of this optimization problem is, unfortunately, not possible, so that iterative methods must be used. The calculations, which have to be performed for each iteration step, consist basically of two parts (cf. 17):

1. calculation of the **descent direction** $p_k \in \mathbb{R}^m$, $p_k \neq 0$;
2. calculation of the **step length** $\alpha_k > 0$, for which we have

$$F(\psi^k + \alpha_k p_k) < F(\psi^k), \tag{6}$$

where ψ^k is the kth element of the iteration sequence. The next sequence element is then defined by

$$\psi^{k+1} := \psi^k + \alpha_k p_k. \tag{7}$$

Thus, the Newton method, for example, uses $p_k = -\mathbf{H}(\psi_k)^{-1}g(\psi_k)$ as descent direction (Newton direction) and $\alpha_k = 1$ as step length, where $\mathbf{H}$ is the positive definite Hesse matrix and g the gradient of the objective function F.

For optimization problems with constraints, additional calculations must be performed to ensure that the elements in the iteration sequence do not violate the constraints.

The LRI Method

The Linear Regression Iteration (LRI) method is a modification of Powell's multidimensional successive-line-minimization method adapted to the YNSN model. In contrast to Powell's method, the minimum search along the straight line is not performed iteratively (cf. 14), but can be chosen optimally with a simple formula. This option likewise considers the constraints.

Descent Direction of the LRI Method

The descent direction p_k in each iteration is chosen along the colorant axes, i.e., the unit vectors $e_i \in \mathbb{R}^m$, (cf. Fig. 1):

$$\begin{aligned} p_0 &:= \pm e_1 \\ p_1 &:= \pm e_2 \\ &\vdots \\ p_{m-1} &:= \pm e_m \end{aligned}$$

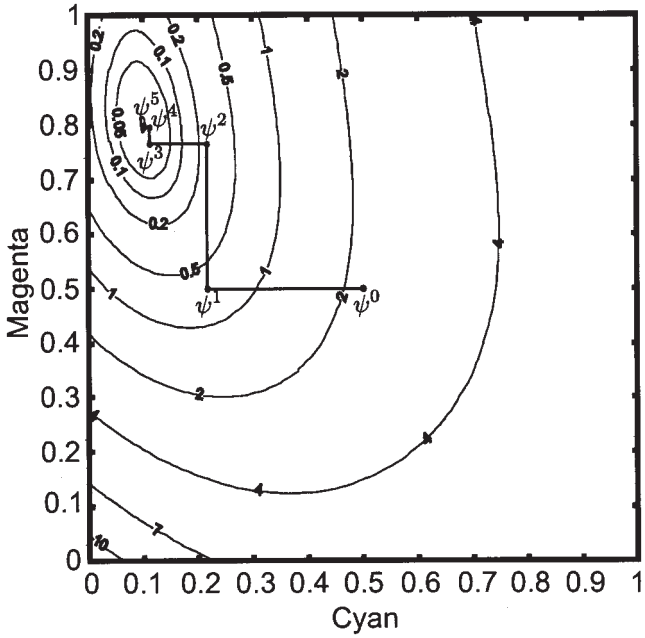

FIG. 1. Level curves of the objective function $F(\psi)$ of a printer with the two colorants cyan and magenta. Plotted are five iteration steps of the LRI method.

$$\text{and } \forall\, k \in \mathbb{N}\colon p_k := \pm e_{(k \bmod m)+1}.$$

Step Length of the LRI Method

We shall show, for the YNSN model, that along the directions in Section 3.1.1, the step length α_k for the objective function (4) can be chosen optimally in each iteration step, i.e.,

$$F(\psi^k + \alpha_k p_k) = \min_{x \in [0,1]} F(\psi_1^k, \ldots, \psi_{(k \bmod m)}^k, x, \psi_{(k \bmod m)+2}^k, \ldots, \psi_m^k). \tag{8}$$

We therefore use the affine multilinearity of the YNSN model in $1/n$-space, i.e., $\forall i \in \{1, \ldots, m\}$:

$$R_\lambda(\psi)^{1/n} = A_{i,\lambda}(\psi) \cdot \psi_i + B_{i,\lambda}(\psi), \tag{9}$$

where $A_{i,\lambda}$ and $B_{i,\lambda}$ hold

$$\frac{\partial A_{i,\lambda}(\psi)}{\partial \psi_i} = \frac{\partial B_{i,\lambda}(\psi)}{\partial \psi_i} = 0. \tag{10}$$

Equation (10) means nothing other than the vector-valued functions $A_{i,\lambda}(\psi)$ and $B_{i,\lambda}(\psi)$ being constant in ψ_i.

We can transform this continuous formulation into a discrete one by sampling all the spectra on $N \in \mathbb{N}$ equidistant wavelengths. The YNSN has the following discrete form in $1/n$-space:

$$\mathbf{R}(\psi) := (R_{\lambda_1}(\psi)^{1/n}, \ldots, R_{\lambda_N}(\psi)^{1/n})^T \tag{11}$$

$$= \sum_{i=1}^{2^m} a_i(\psi) \underbrace{(R_{i,\lambda_1}^{1/n}, \ldots, R_{i,\lambda_N}^{1/n})^T}_{=:\mathbf{R}_i \in [0,1]^N} \tag{12}$$

$$= \sum_{i=1}^{2^m} a_i(\psi)\mathbf{R}_i \tag{13}$$

$$\overset{(9)}{=} \mathbf{A}_i(\psi)\cdot\psi_i + \mathbf{B}_i(\psi), \tag{14}$$

where $\mathbf{A}_i$ and $\mathbf{B}_i$ hold (see Eq. (10)),

$$\frac{\partial \mathbf{A}_i(\psi)}{\partial \psi_i} = \frac{\partial \mathbf{B}_i(\psi)}{\partial \psi_i} = 0. \tag{15}$$

Example 1. For CMY printing, the YNSN model, for example, can be restructured for the colorant cyan as follows:

$$\begin{aligned}
R_\lambda(\psi_c, \psi_m, \psi_y)^{1/n} &= \sum_{i=1}^{2^m} a_i(\psi_c, \psi_m, \psi_y)\, R_{i,\lambda}^{1/n} \\
&= [-(1-\psi_m)(1-\psi_y)R_{1,\lambda}^{1/n} + (1-\psi_m)(1-\psi_y)R_{2,\lambda}^{1/n} - \\
&\quad \psi_m(1-\psi_y)R_{3,\lambda}^{1/n} - (1-\psi_m)\psi_y R_{4,\lambda}^{1/n} - \psi_m\psi_y R_{5,\lambda}^{1/n} + \\
&\quad \underbrace{(1-\psi_m)\psi_y R_{6,\lambda}^{1/n} + \psi_m(1-\psi_y)R_{7,\lambda}^{1/n} + \psi_m\psi_y R_{8,\lambda}^{1/n}]\cdot\psi_c}_{=:\mathbf{A}_c(\psi_m,\psi_y)} + \\
&\quad [(1-\psi_m)(1-\psi_y)R_{1,\lambda}^{1/n} + \psi_m\psi_y R_{5,\lambda}^{1/n} + \\
&\quad \underbrace{\psi_m(1-\psi_y)R_{3,\lambda}^{1/n} + (1-\psi_m)\psi_y R_{4,\lambda}^{1/n}]}_{=:\mathbf{B}_c(\psi_m,\psi_y)} \\
&= \mathbf{A}_c(\psi_m,\psi_y)\cdot\psi_c + \mathbf{B}_c(\psi_m,\psi_y).
\end{aligned}$$

Analogously, the model can be transformed also for magenta and yellow.

When the YNSN model has been put into the form from Eq. (14), the following overdetermined equation system,

$$\mathbf{A}_i(\psi)\cdot\psi_i + \mathbf{B}_i(\psi) = \mathbf{r}, \tag{16}$$

with the discretized reflectance spectrum $\mathbf{r} = (r_{\lambda_1}^{1/n}, \ldots, r_{\lambda_N}^{1/n})^T$ to be reproduced can be solved for ψ_i by means of linear regression:

$$\psi_i^{\min} \equiv \frac{\mathbf{A}_i^T(\psi)\cdot(\mathbf{r} - \mathbf{B}_i(\psi))}{\mathbf{A}_i^T(\psi)\cdot\mathbf{A}_i(\psi)}. \tag{17}$$

The so determined $\psi_i^{\min}$ is the optimal solution in the sense of the smallest RMS error, i.e.,

$$\min_{\psi_i\in\mathbb{R}} \|\mathbf{R}(\psi) - \mathbf{r}\|_2^2 = \|\mathbf{R}(\psi_1, \ldots, \psi_i^{\min}, \ldots, \psi_m) - \mathbf{r}\|_2^2. \tag{18}$$

The affine multilinearity of the YNSN model in the $1/n$-space permits very straightforward accommodation of the constraints

$$\bar{\psi}_i^{\min} = \begin{cases} 0, & \psi_i^{\min} < 0 \\ \psi_i^{\min}, & \psi_i^{\min} \in [0,1] \\ 1, & \psi_i^{\min} > 1. \end{cases} \tag{19}$$

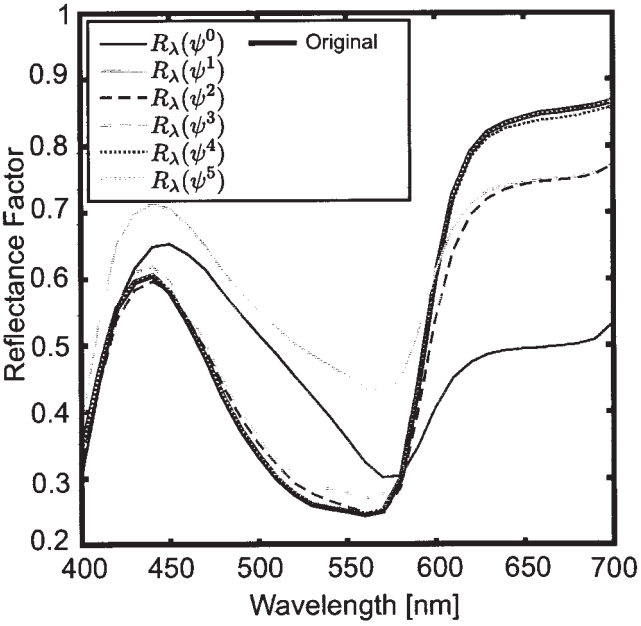

FIG. 2. Corresponding reflectance spectra (gray lines) of each iteration from Fig. 1. Original spectrum (black line).

The so-chosen $\bar{\psi}_i^{\min}$ is the solution of the constrained problem, i.e.,

$$\min_{\psi_i\in[0,1]} \|\mathbf{R}(\psi) - \mathbf{r}\|_2^2 = \|\mathbf{R}(\psi_1, \ldots, \bar{\psi}_i^{\min}, \ldots, \psi_m) - \mathbf{r}\|_2^2. \tag{20}$$

From this follows, for the descent direction of the kth iteration step,

$$p_k := \frac{\bar{\psi}_{(k \bmod m)+1}^{\min} - \psi_{(k \bmod m)+1}^k}{|\bar{\psi}_{(k \bmod m)+1}^{\min} - \psi_{(k \bmod m)+1}^k|}\cdot e_{(k \bmod m)+1} \tag{21}$$

and for the optimal step length,

$$\alpha_k := |\bar{\psi}_{(k \bmod m)+1}^{\min} - \psi_{(k \bmod m)+1}^k|. \tag{22}$$

Descent direction (21) and step length (22) have been so defined that the $k+1$ sequence element according to Eq. (7) just forms the solution of the one-dimensional problem (20). We may write

$$\psi^{k+1} = \psi^k + \alpha_k p_k = (\psi_1^k, \ldots, \bar{\psi}_{(k \bmod m)+1}^{\min}, \ldots, \psi_m^k)^T. \tag{23}$$

The LRI method converges to a limiting value satisfying the necessary condition that a solution of the discretized problem 1 must meet (cf. Appendix A).

Figures 1 and 2 illustrate the LRI method using, as an example, a printer with the colorants cyan and magenta.

Algorithm

The LRI algorithm may be written in the following simple form without explicitly stating the descent direction and step length:

1. $\psi = (0.5, \ldots, 0.5)^T$
2. REPEAT {
3. FOR ($i = 1$; $i \leq m$; $i = i + 1$)
4. {
5. $\psi_i = \dfrac{\mathbf{A}_i^T(\psi)\cdot(r - B_i(\psi))}{\mathbf{A}_i^T(\psi)\mathbf{A}_i(\psi)}$;
6. IF ($\psi_i < 0$) {$\psi_i = 0$};
7. IF ($\psi_i > 1$) {$\psi_i = 1$};
8. }
9. } UNTIL Termination

Appendix B contains a complexity estimation of the method and a few hints for an effective implementation. It is shown that an iteration step essentially consists of two matrix–vector multiplications.

Termination Criteria

If it is desired that the value of the objective function at the point ψ^k found correspond to the actual minimum value of the first q-decimal places, then Gill *et al.*[17] suggest, among other things, the following termination criteria, with $\tau := 10^{-q}$

C1: $F(\psi^{k-m}) - F(\psi^k) \leq \tau(1 + F(\psi^k))$
C2: $\|\psi^{k-m} - \psi^k\| \leq \sqrt{\tau}(1 + \|\psi^k\|)$
C3: $k \geq k_{\max}$.

Termination is to be effected when **C1** *and* **C2** are satisfied *or* when condition **C3** occurs, where $k_{\max}$ is a maximum number of iteration steps chosen by the user.

EXPERIMENTS

The objective of the following simulation experiments shall be the estimation of the speed of convergence of the LRI method. The authors stress that the question of the performance of the YNSN model as an estimator of printed reflectance spectra is not the subject of this article. In this respect, reference is made, e.g., to Rolleston and Balasubramanian[10] or Wyble and Berns.[9]

For the simulation we used YNSN models of a CMYKOG printer with various Yule–Nielsen n-factors and with the colorant reflectance spectra shown in Fig. 3. For the LRI method, three different τ-factors are used controlling the termination conditions (cf. Section 3.2.1). In each simulation, the mean and maximum number of iteration steps and the mean and maximum RMS error are to be determined as a function of the Yule–Nielsen n-factors as well as of the termination factor τ.

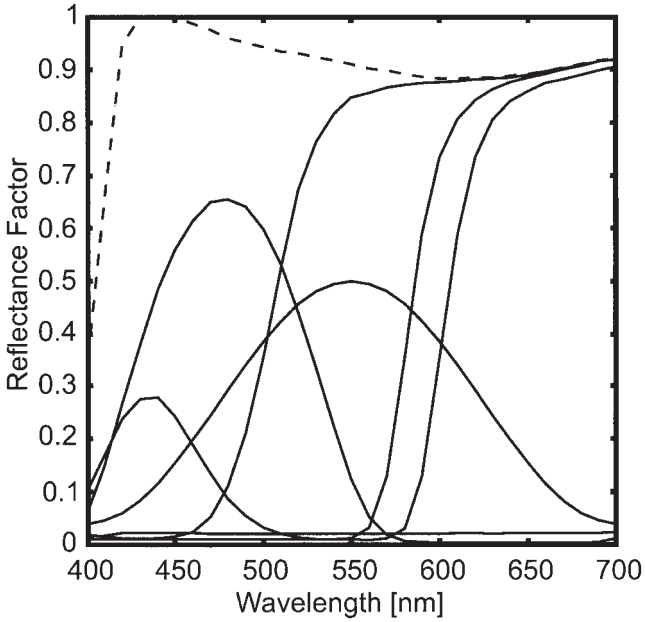

FIG. 3. Reflectance spectra (solid lines) of the colorants and paper white (dashed line) used for the simulation.

In Simulation I, the reflectance spectra of

$$(C, M, Y, K, O, G)^T \in \{0, 0.2, 0.4, 0.6, 0.8, 1\}^6 \quad (24)$$

are determined via the YNSN model. These reflectance spectra, by their design lying within the spectral gamut of the printer, serve as input for the LRI method.

In practice, reflectance spectra not lying within the spectral gamut of the printer must be considered. A frequent application is the separation of a multispectral image with out-of-gamut spectra, which is addressed in Simulation II. For this, use is made of the reflectance spectra of two multispectral images of real-world scenes (cf. Fig. 4). The images are part of a database of multispectral images, freely available for scientific purposes, which are published on the website of the University of Joensuu, Finland (*http://spectral.joensuu.fi/*) (cf. 25).

In the separation of real-world multispectral images, use can be made of the generally high correlation of neighboring pixels. Where separation is computed for a pixel, it may be assumed that neighboring pixels have a similar separation of the colorants. In this simulation, the reflectance spectra of each image are arranged by columns and the separation of the previous pixel used as start value of the current pixel.

TABLE I. Simulation parameters.

	Simulation I	Simulation II
Yule–Nielsen n-factors	1.0, 1.5, . . . , 5.0	1.0, 1.5, . . . , 5.0
Termination τ-factors	10^{-3}, 10^{-4}, 10^{-5}	10^{-3}, 10^{-4}, 10^{-5}
Test spectra	6^6 spectra inside the spectral gamut	*YoungGirl* (12789 pixel) *YarnPalette* (983735 pixel)
Spectral sampling [nm]	400, 410, . . . , 700	400, 410, . . . , 700

FIG. 4. The multispectral images used in Simulation II transformed to sRGB: (a) *Young Girl* (147 × 87 pixels); (b) *Yarn Palette* (905 × 1087 pixels) (copyright by Color AIXperts GmbH).

The simulation parameters of both simulations are summarized in Table I.

RESULTS AND DISCUSSION

The results of Simulation I are summarized for $n = 1, 3, 5$ in Table II and in terms of color differences for the CIE illuminants A (incandescent light), C (average daylight), and F11 (fluorescent lamp) in Table III. Figure 5 shows the number of iteration steps as a function of the Yule–Nielsen n-factor for the three termination factors τ investigated. Figure 6 shows the corresponding RMS errors, which will shrink with increasing n-factors. This is due to the separation computation being conducted in the $1/n$-space, whereas the RMS error is determined based on the actual reflectance spectra. An RMS error of reflectance spectra in the $1/n$-space ($n > 1$), as used, e.g., in the termination condition **C1** (cf. Section on Step Length), in the actual space, i.e., by raising each component of the reflectance spectra to the n power, generally becomes smaller with increasing n (an exception are reflectance spectra with intensities near 1).

Reference is made here to a further interesting effect: For $\tau = 10^{-3}$, the ink combinations found deviate clearly in part from the ink combinations used in the simulation to generate the reflectance spectrum to be reproduced (cf. sample set of inks (24)). Still, the RMS does not differ, on an average, from the other separations, which underlines the results of Rosen *et al.*[26] on spectral redundance in six ink color printers.

The choice of $\tau = 10^{-4}$ seems a good compromise between computational effort (approx. 60 iterations on an average) and RMS accuracy (approx. 0.01). At n-factors near 1, a somewhat smaller τ-value should be used.

The results of Simulation II are summarized in Table IV for the image *Young Girl* and in Table V for the image *Yarn Palette,* in each case for $n = 1, 3, 5$. Figure 7 shows the mean number of iterations and Fig. 8 the mean RMS errors.

As there are also out-of-gamut spectra in the images, the mean RMS errors are significantly higher than in Simulation I. Exactly as in Simulation I this experiment, too, shows that, for increasing n-factors, the RMS error will drop. This again is due to computing the separation in the $1/n$-space.

Utilization of the correlation in the images is reflected in a significant reduction of the iteration steps, which, in the

TABLE II. Results for Simulation I.

		Iterations			RMS		
n	τ	Mean	Std	Max	Mean	Std	Max
1	10^{-3}	21.1	18.7	186	0.035	0.031	0.223
	10^{-4}	58.2	56.2	576	0.020	0.017	0.110
	10^{-5}	168.8	155.7	1518	0.009	0.008	0.047
3	10^{-3}	26.6	18.3	144	0.017	0.025	0.237
	10^{-4}	68.0	43.3	648	0.007	0.010	0.111
	10^{-5}	149.5	122.7	1428	0.003	0.004	0.047
5	10^{-3}	27.0	16.2	144	0.015	0.028	0.291
	10^{-4}	69.7	37.4	540	0.007	0.011	0.155
	10^{-5}	148.5	119.0	1416	0.003	0.005	0.061

TABLE III. Colorimetric results for Simulation I.

		ΔE_{ab}, A			ΔE_{ab}, C			ΔE_{ab}, F11		
n	τ	Mean	Std	Max	Mean	Std	Max	Mean	Std	Max
1	10^{-3}	2.7	2.1	46.7	2.8	2.2	66.3	3.2	2.5	58.4
	10^{-4}	1.4	1.3	22.1	1.5	1.3	22.8	1.7	1.5	25.4
	10^{-5}	0.7	0.8	17.5	0.7	0.8	18.6	0.8	0.9	20.7
3	10^{-3}	1.6	1.1	8.3	1.5	1.1	10.5	1.8	1.4	9.2
	10^{-4}	0.7	0.4	4.3	0.6	0.4	3.5	0.8	0.6	6.6
	10^{-5}	0.3	0.2	1.3	0.2	0.2	1.5	0.3	0.3	2.5
5	10^{-3}	1.5	1.3	8.5	1.4	1.3	9.9	1.7	1.6	10.1
	10^{-4}	0.6	0.5	4.1	0.6	0.5	3.5	0.8	0.7	6.1
	10^{-5}	0.2	0.2	1.5	0.2	0.2	1.4	0.3	0.3	3.0

case of the *Yarn Palette* image, are only about half the iterations that could be observed in Simulation I. This image shows moreover that $\tau = 10^{-5}$ hardly yields an RMS advantage compared to $\tau = 10^{-4}$ (cf. Fig. 8), but nearly doubles the number of iteration steps (cf. Fig. 7).

CONCLUSION

This paper has presented a simple method for the iterative inversion of the YNSN model. The method utilizes the affine multilinearity of the YNSN model in the $1/n$-space to determine by means of linear regression, in each iteration step, the exact minimum, with respect to the RMS error, along a colorant axis. The iteration converges to a colorant combination in the colorant space, which generates a reflectance spectrum having the smallest RMS error regarding the reproducible reflectance spectrum. Simulation experiments using a CMYKOG color printer showed a mean iteration number of approx. 60 for sufficiently accurate reproduction for most applications, using an in-gamut reflectance spectrum. Further simulation experiments showed that this value can be reduced significantly utilizing the correlations in real-world multispectral images.

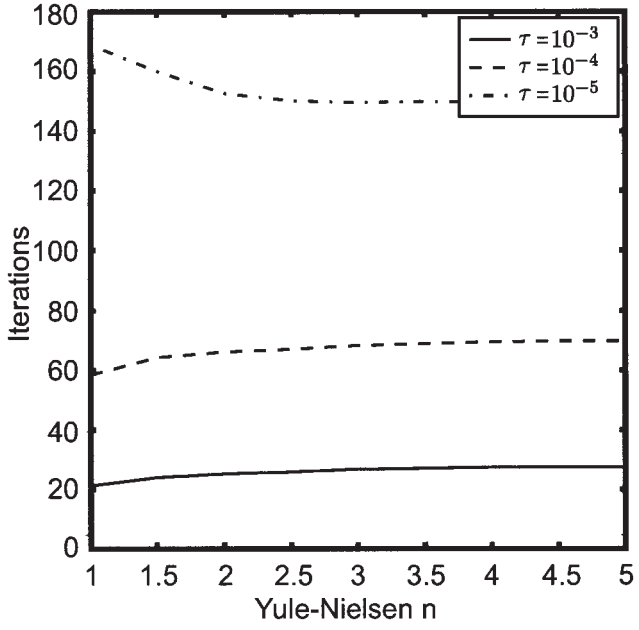

FIG. 5. Mean number of iteration steps in Simulation I for various termination factors τ as a function of the Yule–Nielsen n-factor.

APPENDIX A

Mathematical Background

In this section we will consider the discretized form of the constrained optimization Problem 1 from the section on Inversion.

Problem 2.

Solve

$$\mathbf{F}(\psi) := \|\mathbf{R}(\psi) - \mathbf{r}\|_2^2 = \sum_{j=1}^{N} (\mathbf{R}_j(\psi) - \mathbf{r}_j)^2 \overset{!}{=} \min \quad (25)$$

with the constraint

$$\psi \in [0, 1]^m. \quad (26)$$

We will show that a minimum of Problem 2 must satisfy a necessary condition, which is met by the limiting value of the LRI method.

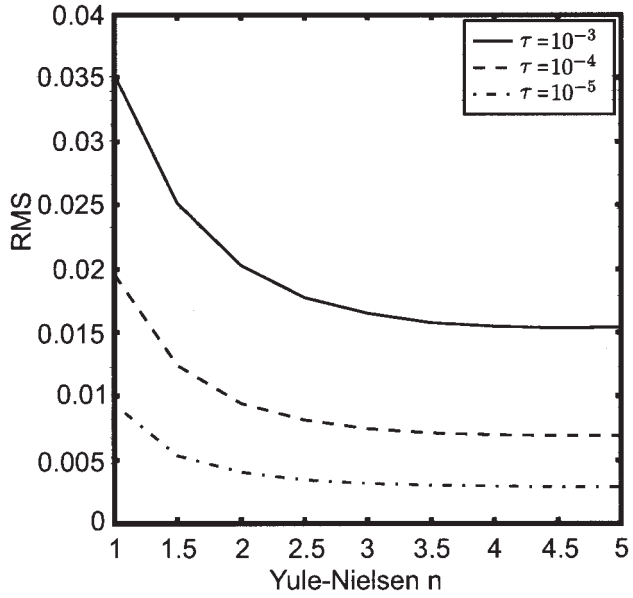

FIG. 6. Mean RMS error in Simulation I for various termination factors τ as a function of the Yule–Nielsen n-factor.

TABLE IV. Results for Simulation II, Image: *Young Girl.*

		Iterations			RMS		
n	τ	Mean	Std	Max	Mean	Std	Max
1	10^{-3}	16.1	13.7	222	0.187	0.088	0.380
	10^{-4}	42.2	58.3	504	0.171	0.095	0.378
	10^{-5}	104.0	145.8	1374	0.168	0.097	0.377
3	10^{-3}	14.3	11.7	198	0.163	0.091	0.382
	10^{-4}	38.8	53.0	540	0.150	0.093	0.382
	10^{-5}	112.6	129.1	912	0.145	0.095	0.382
5	10^{-3}	12.2	8.8	174	0.159	0.093	0.384
	10^{-4}	28.9	42.4	450	0.149	0.094	0.384
	10^{-5}	86.9	105.0	756	0.143	0.096	0.384

Theorem 1 (*Necessary Condition*)
If $\psi^* = (\psi_1^*, \ldots, \psi_m^*)^T$ be the local minimum of Problem 2, then the following conditions hold for all $i = 1, \ldots, m$:

$$\psi_i^* = \begin{cases} 0, & \psi_i^{\min} < 0 \\ \psi_i^{\min}, & \psi_i^{\min} \in [0, 1], \\ 1, & \psi_i^{\min} > 1 \end{cases} \quad \text{where} \quad \psi_i^{\min} = \frac{\mathbf{A}_i^T(\psi^*) \cdot (\mathbf{r} - \mathbf{B}_i(\psi^*))}{\mathbf{A}_i^T(\psi^*) \cdot \mathbf{A}_i(\psi^*)}. \tag{27}$$

Proof. We will first consider the unconstrained problem, computing the partial derivations from **F:**

$$\frac{\partial \mathbf{F}(\psi)}{\partial \psi_i} = 2 \cdot \sum_{j=1}^{N} (\mathbf{R}_j(\psi) - \mathbf{r}_j) \cdot \frac{\partial \mathbf{R}_j(\psi)}{\partial \psi_i} \tag{28}$$

$$\overset{(14)}{=} 2 \cdot \sum_{j=1}^{N} (\mathbf{R}_j(\psi) - \mathbf{r}_j) \cdot \mathbf{A}_{i_j}(\psi) \tag{29}$$

$$\overset{(14)}{=} 2 \cdot \sum_{j=1}^{N} (\mathbf{A}_{i_j}(\psi) \cdot \psi_i + \mathbf{B}_{i_j}(\psi) - \mathbf{r}_j) \cdot \mathbf{A}_{i_j}(\psi) \tag{30}$$

$$= 2\psi_i \cdot [\sum_{j=1}^{N} (\mathbf{A}_{i_j}(\psi))^2] + 2 \cdot [\sum_{j=1}^{N} \mathbf{A}_{i_j}(\psi) \cdot (\mathbf{B}_{i_j}(\psi) - \mathbf{r}_j)] \tag{31}$$

$$= 2\psi_i \cdot \mathbf{A}_i^T(\psi)\mathbf{A}_i(\psi) + 2 \cdot \mathbf{A}_i^T(\psi)(\mathbf{B}_i(\psi) - \mathbf{r}). \tag{32}$$

Therefore, the following equivalence applies considering $\mathbf{A}_i(\psi) \neq 0$,

$$\psi_i = \frac{\mathbf{A}_i^T(\psi)(\mathbf{r} - \mathbf{B}_i(\psi))}{\mathbf{A}_i^T(\psi)\mathbf{A}_i(\psi)} \Leftrightarrow \frac{\partial \mathbf{F}(\psi)}{\partial \psi_i} = 0. \tag{33}$$

For the fixed point

$$\psi = (\psi_1, \ldots, \psi_m)^T = \left(\frac{\mathbf{A}_1^T(\psi)(\mathbf{r} - \mathbf{B}_1(\psi))}{\mathbf{A}_1^T(\psi)\mathbf{A}_1(\psi)}, \ldots, \frac{\mathbf{A}_m^T(\psi)(\mathbf{r} - \mathbf{B}_m(\psi))}{\mathbf{A}_m^T(\psi)\mathbf{A}_m(\psi)} \right)^T \tag{34}$$

we can write

$$\nabla \mathbf{F}\left(\frac{\mathbf{A}_1^T(\psi)(\mathbf{r} - \mathbf{B}_1(\psi))}{\mathbf{A}_1^T(\psi)\mathbf{A}_1(\psi)}, \ldots, \frac{\mathbf{A}_m^T(\psi)(\mathbf{r} - \mathbf{B}_m(\psi))}{\mathbf{A}_m^T(\psi)\mathbf{A}_m(\psi)} \right) = 0. \tag{35}$$

This point satisfies, according to Ref. 17, the necessary condition of the first order for the unconstrained optimization problem.

If we now consider a local solution ψ^* of the constrained optimization problem 2, then this is also a local solution for the following problem.

Problem 3.

TABLE V. Results for **Simulation II,** Image: *Yarn Palette.*

		Iterations			RMS		
n	τ	Mean	Std	Max	Mean	Std	Max
1	10^{-3}	12.2	14.4	1188	0.166	0.144	0.999
	10^{-4}	32.3	51.5	2082	0.161	0.144	0.999
	10^{-5}	82.0	139.1	3228	0.160	0.144	0.999
3	10^{-3}	15.9	17.8	474	0.159	0.147	1.043
	10^{-4}	39.2	47.2	1398	0.158	0.147	1.042
	10^{-5}	76.5	100.5	3510	0.158	0.147	1.041
5	10^{-3}	15.0	19.7	4284	0.160	0.149	1.159
	10^{-4}	39.4	59.7	5466	0.158	0.149	1.159
	10^{-5}	77.9	126.8	5946	0.158	0.148	1.157

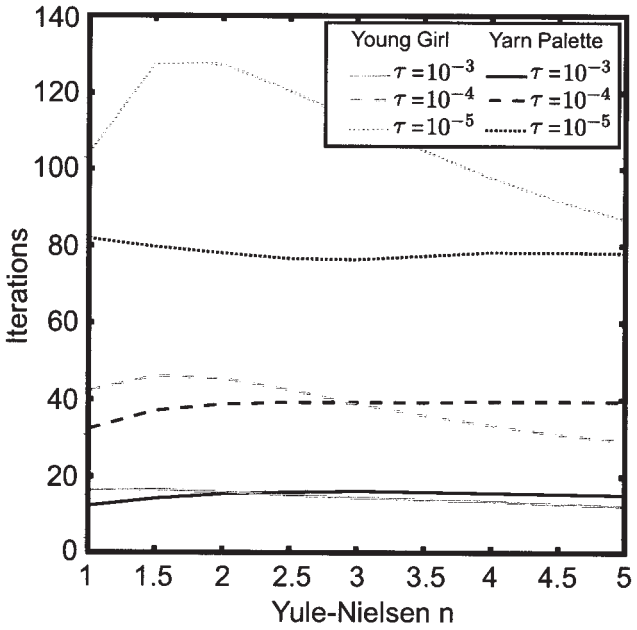

FIG. 7. Mean number of iteration steps in Simulation II for various termination factors τ as a function of the Yule–Nielsen n-factor.

$$\mathbf{F}(\psi) := \|\mathbf{R}(\psi) - \mathbf{r}\|_2^2 = \sum_{j=1}^{N} (\mathbf{R}_j(\psi) - \mathbf{r}_j)^2 \stackrel{!}{=} \min \quad (36)$$

with the constraints

$$\psi_i = 0, \quad i \in J_0 = \{i \in \{1, \ldots, m\} | \psi_i^* = 0\} \quad (37)$$

$$\psi_j = 1, \quad j \in J_1 = \{i \in \{1, \ldots, m\} | \psi_i^* = 1\}, \quad (38)$$

where J_0 and J_1 form the index set of the inequality constraints active in ψ^*. The associated ψ_i, $i \in J_0 \cup J_1$ accordingly are fixed, with the solution lying on the associated hyperplane. The necessary condition of the first order for a minimum on this hyper plane reads

$$\frac{\partial \mathbf{F}(\psi)}{\partial \psi_i} = 0, \quad \forall\, i \notin J_0 \cup J_1 \quad (39)$$

$$\stackrel{(33)}{\Leftrightarrow} \psi_i = \frac{\mathbf{A}_i^T(\psi)(\mathbf{r} - \mathbf{B}_i(\psi))}{\mathbf{A}_i^T(\psi)\mathbf{A}_i(\psi)}, \quad \forall\, i \notin J_0 \cup J_1, \quad (40)$$

where $\psi_j = 0$, $j \in J_0$ and $\psi_j = 1$, $j \in J_1$ are constant. Hence, we have

$$0 \le \psi_i^* = \frac{\mathbf{A}_i^T(\psi^*) \cdot (\mathbf{r} - \mathbf{B}_i(\psi^*))}{\mathbf{A}_i^T(\psi^*) \cdot \mathbf{A}_i(\psi^*)} \le 1, \quad \forall\, i \notin J_0 \cup J_1. \quad (41)$$

As ψ^*, by way of assumption, is the minimum of Problem 2, we will, with a little computing, obtain from the affine multilinearity of $\mathbf{R}(\psi)$:

$$\frac{\mathbf{A}_i^T(\psi^*) \cdot (\mathbf{r} - \mathbf{B}_i(\psi^*))}{\mathbf{A}_i^T(\psi^*) \cdot \mathbf{A}_i(\psi^*)} \begin{cases} \le 0, & \forall\, i \in J_0, \\ \ge 1, & \forall\, i \in J_1. \end{cases} \quad (42)$$

The design of the LRI method leads to a limiting value that meets the necessary condition from Theorem 1.

Ensured, incidentally, is the convergence of the LRI method since a sequence $F(\psi^i) \ge F(\psi^{i+1})$ bounded below and monotonically decreasing converges to its infimum.

APPENDIX B

Complexity Estimation and Recommendations for Implementation

This Section is to determine the complexity of an iteration step of the **LRI** method with respect to multiplication operations and to make some recommendations as to what an efficient implementation could look like. Basis of an iteration step is the determination of $\psi_i^{\min}$ with the aid of the formula from Eq. (17):

$$\psi_i^{\min} \equiv \frac{\mathbf{A}_i^T(\psi) \cdot (\mathbf{r} - \mathbf{B}_i(\psi))}{\mathbf{A}_i^T(\psi) \cdot \mathbf{A}_i(\psi)}. \quad (43)$$

The vectors $\mathbf{A}_i(\psi)$, $\mathbf{B}_i(\psi)$, $i \in 1, \ldots, m$ can each be expressed as a multiplication of a constant $N \times 2^{m-1}$ matrix $\mathbf{A}_i$ or $\mathbf{B}_i$ and a vector $\mathbf{v}_i(\psi) \in \mathbb{R}^{(2^{m-1})}$, i.e.,

$$\mathbf{A}_i(\psi) = \mathbf{A}_i \cdot \mathbf{v}_i(\psi) \quad (44)$$

$$\mathbf{B}_i(\psi) = \mathbf{B}_i \cdot \mathbf{v}_i(\psi). \quad (45)$$

The vector $\mathbf{v}_i(\psi)$ must be newly computed for each iteration step, which, for a printer with m colorants, can be done as follows:

$$w_1(\psi) = \begin{bmatrix} 1 \\ \psi_{i_1} \end{bmatrix}, \quad (46)$$

$$w_2(\psi) = \begin{bmatrix} w_1(\psi) \\ \psi_{i_2} \cdot w_1(\psi) \end{bmatrix}, \quad (47)$$

$$\vdots \quad (48)$$

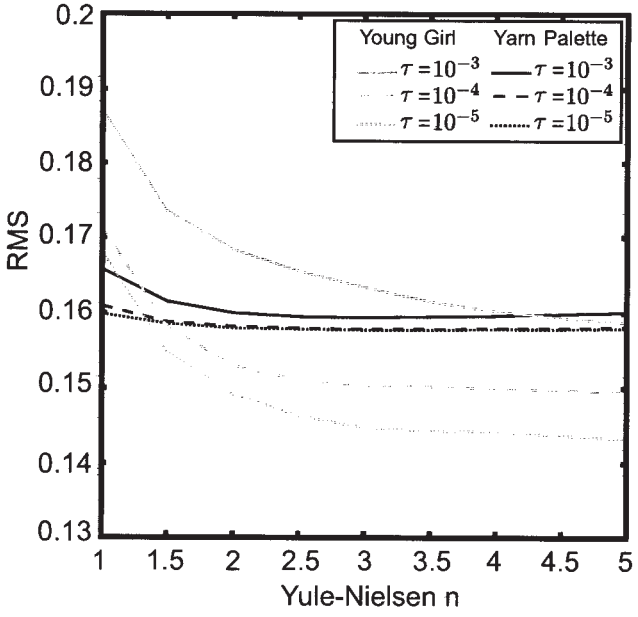

FIG. 8. Mean RMS errors in Simulation II for various termination factors τ as a function of the Yule–Nielsen n-factor.

$$w_{m-1}(\psi) = \begin{bmatrix} w_{m-2}(\psi) \\ \psi_{i_{m-1}} \cdot w_{m-2}(\psi) \end{bmatrix} =: \mathbf{v}_i(\psi) \qquad (49)$$

with $i_j < i_{j+1}$ and $i_j \neq i$.

Each calculation of $\mathbf{v}_i(\psi)$ requires $2^1 + 2^2 + \cdots + 2^{m-2}$ multiplications. The matrices $\mathbf{A}_i$, $\mathbf{B}_i$, $i \in 1, \ldots, m$, for a fitted YNSN model, must only be determined once. The matrix entries may simply be obtained from the form in Eq. (14) after all weights have been expanded.

Example 2. For **Example 1,** the matrices $\mathbf{A}_c$, $\mathbf{B}_c$ and the vector $\mathbf{v}_c$ can be stated as

$$\mathbf{A}_c = \begin{bmatrix} (-R_{1,\lambda}^{1/n} + R_{2,\lambda}^{1/n})^T \\ (R_{1,\lambda}^{1/n} - R_{2,\lambda}^{1/n} - R_{3,\lambda}^{1/n} + R_{7,\lambda}^{1/n})^T \\ (R_{1,\lambda}^{1/n} - R_{2,\lambda}^{1/n} - R_{4,\lambda}^{1/n} + R_{6,\lambda}^{1/n})^T \\ (-R_{1,\lambda}^{1/n} + R_{2,\lambda}^{1/n} + R_{3,\lambda}^{1/n} + R_{4,\lambda}^{1/n} - R_{5,\lambda}^{1/n} - R_{6,\lambda}^{1/n} - R_{7,\lambda}^{1/n} + R_{8,\lambda}^{1/n})^T \end{bmatrix}^T, \qquad (50)$$

$$\mathbf{B}_c = \begin{bmatrix} (R_{1,\lambda}^{1/n})^T \\ (-R_{1,\lambda}^{1/n} + R_{3,\lambda}^{1/n})^T \\ (-R_{1,\lambda}^{1/n} + R_{4,\lambda}^{1/n})^T \\ (R_{1,\lambda}^{1/n} + R_{5,\lambda}^{1/n} - R_{3,\lambda}^{1/n} - R_{4,\lambda}^{1/n})^T \end{bmatrix}^T, \quad \mathbf{v}_c = \begin{bmatrix} 1 \\ \psi_m \\ \psi_y \\ \psi_m \psi_y \end{bmatrix}. \qquad (51)$$

In the two matrix–vector multiplications for computation of the vectors $\mathbf{A}_i(\psi)$ and $\mathbf{B}_i(\psi)$, $i \in 1, \ldots, m$, each iteration step once more requires $2(N \cdot 2^{m-1})$ multiplications.

To calculate the formula in Eq. (17), two scalar products have yet to be determined requiring N multiplications each.

In total, the number of multiplication operations $\mathcal{N}(N, m)$ for an iteration step may be stated as

$$\mathcal{N}(N, m) = \underbrace{2^1 + 2^2 + \cdots + 2^{m-2}}_{\mathbf{v}_i(\psi)} + \underbrace{2(N \cdot 2^{m-1})}_{\begin{matrix}\mathbf{A}_i(\psi) \\ \mathbf{B}_i(\psi)\end{matrix}} + \underbrace{2N}_{\begin{matrix}\mathbf{A}_i^T(\psi) \cdot (\mathbf{r} - \mathbf{B}_i(\psi)) \\ \mathbf{A}_i^T(\psi) \cdot \mathbf{A}_i(\psi)\end{matrix}}. \qquad (52)$$

The complexity of each iteration step regarding multiplication operations as a function of the spectral sampling rate N is $\mathbb{O}(N)$ and, regarding the number of colorants m, $\mathbb{O}(2^m)$. Accordingly, increase of the spectral sampling rate is relatively unproblematic for the runtime performance. Every further additional colorant, however, will double the number of multiplication operations.

The spectral separation for $m = 6$ colorants and a spectral sampling of $N = 31$ (cf. the simulation experiments in Experiments Section) requires 2076 multiplications in each iteration step.

As by far the largest part of multiplication operations is accounted for by the matrix–vector multiplications, the runtime optimization of this part is of particular importance. To be recommended here is the use of special optimized software, such as Basic Linear Algebra Subprograms (BLAS) (see, e.g., *http://www.netlib.org/blas*). The BLAS library has been adapted by various microprocessor manufacturers (e.g., Intel and AMD) to their current hardware, enabling partially parallel computation on standard processors available today.

1. Murray A. Monochrome reproduction in photoengraving. J Franklin Inst 1936;221:721–744.
2. Neugebauer HEJ. Die theoretischen grundlagen des mehrfarbenbuchdrucks. Zeit wissenschaft Photogr Photophys Photochem [reprinted in 27, translated in 28] 1937;36:73–89.
3. Yule JAC, Nielsen WJ. The penetration of light into paper and its effect on halftone reproduction. J Tech Assoc Graphic Arts 1951;4:65–76.
4. Arney J, Engeldrum P, Zeng H. An expanded Murray–Davies model of tone reproduction in halftone imaging. IS&T Recent Prog Dig Halftoning II 1999;390–396.
5. Yule JAC, Colt RS. Colorimetric investigations in multicolor printing. TAGA Proc 1951;77–82.
6. Heuberger KJ, Jing ZM, Persiev S. Color transformations from lookup tables. TAGA Proc 1992;863–881.
7. Arney JS, Wu T, Blehm C. Modeling the Yule–Nielsen effect on color halftones. J Imaging Sci Technol 1998;42:335–340.
8. Emmel P, Hersch RD. A unified model for color prediction of halftoned prints. J Imaging Sci Technol 2000;44:351–359.
9. Wyble DR, Berns RS. A critical review of spectral models applied to binary color printing. Color Res Appl 2000;25:4–19.
10. Rolleston R, Balasubramanian R. Accuracy of various types of Neugebauer model. Scottsdale, AZ: IS&T/SID: CIC; 1993. pp 32–36.
11. Imai FH, Rosen MR, Berns RS. Comparative study of metrics for spectral match quality. Poitiers, France: IS&T: CGIV; 2002. pp 492–496.
12. Zuffi S, Schettini R. Spectral-based printer characterization. Poitiers, France: IS&T: CGIV; 2002. pp 598–602.
13. Taplin LA. Spectral modeling of a six-color inkjet printer, MSc. thesis. New York: RIT; 2001.
14. Press WH, Flannery BP, Teukilsky SA, Vetterling WT. Numerical recipes in C, Vol 1. Cambridge University Press; 1988.
15. Tzeng DY. Spectral-based color separation algorithm developed for multiple-ink color reproduction, Ph.D. thesis. New York: RIT; 1999.
16. Tzeng DY, Berns RS. Spectral-based six-color separation minimizing metamerism. Scottsdale, AZ: IS&T/SID: CIC; 2000. pp 342–347.
17. Gill PE, Murray W, Wright MH. Practical optimization. Academic Press; 1981.
18. Arney JS. A probability description of the Yule–Nielsen effect. J Imaging Sci Technol 1997;41:633–636.
19. Arney JS, Katsube M. A probability description of the Yule–Nielsen effect. II: The impact of halftone geometry. J Imaging Sci Technol 1997;41:637–642.
20. Arney JS, Yamaguchi S. The physics behind the Yule–Nielsen equation. Savannah, GA: IS&T: PICS; 1999. pp 381–385.
21. Rogers GL. Optical dot gain in a halftone print. J Imaging Sci Technol 1997;41:643–656.
22. Iino K, Berns RS. Building color-management modules using linear optimization I. Desktop Color System. J Imaging Sci Technol 1998;42:79–94.
23. Iino K, Berns RS. Building color-management modules using linear optimization. II. Prepress system for offset printing. J Imaging Sci Technol 1998;42:99–114.
24. Balasubramanian R. Optimization of the spectral Neugebauer model for printer characterization. J Electron Imaging 1999;8:156–166.
25. Kohonen O, Parkkinen J, Jaaskelainen T. Databases for spectral color science. Granada, Spain: AIC Colour 05; 2005. pp 1649–1652.
26. Rosen MR, Hattenberger EF, Ohta N. Spectral redundancy in a six-ink ink jet printer. J Imaging Sci Technol 2004;48:194–202.
27. Neugebauer HEJ. Die theoretischen grundlagen des mehrfarbenbuchdrucks. In: Proceedings of SPIE: Neugebauer Memorial Seminar on Color Reproduction, Tokyo, Japan, 1989. Vol 1184, pp 194–202.
28. Neugebauer HEJ. The theoretical basis of multicolor letterpress printing (translated by D. Wyble and A. Kraushaar). Color Res Appl 2005;30:322–331.